Evaluation of the Complex Hygrothermal Behaviors of Epoxy–Amine Systems

Sungwon Choi, Andrea Phantu, Elliot P. Douglas

Department of Materials Science and Engineering, University of Florida, Gainesville, Florida 32608

Received 14 June 2011; accepted 25 November 2011
DOI 10.1002/app.36539
Published online in Wiley Online Library (wileyonlinelibrary.com).

ABSTRACT: In this study, the complex hygrothermal behavior of two epoxy systems used for strengthening applications was studied. In these systems, property loss by plasticization simultaneously occurred with property gain during additional curing. A comparison of the changes in the glass-transition temperature (T_g) and crosslink density with water immersion at different temperatures clearly showed that the two effects of additional curing by a postcuring reaction and plasticization by water absorption were in competition with each other during the exposure. The changes in the conversion with different exposure conditions suggested that water accelerated the postcuring reaction, even at low temperatures; this resulted in a significant difference in the postcuring reaction between unexposed and exposed epoxies. The construction of the plot of T_g versus conversion for the unexposed system and the placement of the T_g for exposed systems onto this master plot provided a method for evaluating the plasticization effect while excluding the influence of additional curing. © 2012 Wiley Periodicals, Inc. J Appl Polym Sci 000: 000–000, 2012

Key words: differential scanning calorimetry; glass transition; infrared spectroscopy; thermosets

INTRODUCTION

Because epoxies were applied commercially, they have been used extensively for various applications, such as matrices of composite materials, aerospace components, structural adhesives, and reinforcements in civil infrastructure applications; they show outstanding performance with a high strength, stiffness, and resistance to creep.[1–5] In these applications, the performance of epoxy-based composites have been greatly affected by environmental exposure, in which their spontaneous absorption of moisture of up to 7–8 wt % has a detrimental effect on the properties of the epoxies, such as decreases in the tensile strength and modulus, adhesive strength, and glass-transition temperature (T_g).[6–15] For such property losses, the plasticization effect by absorbed water, in which water diffuses into the free volume of the network and causes either an increase in the mobility of the chains or a disruption of interchain hydrogen bonds by water molecules, is considered to be the primary reason.[10,16–20]

However, these detrimental effects often include some complex behavior in that the property increase happens simultaneously with property loss by water plasticization because of an increase in the crosslink density by a postcuring reaction.[15,21–26] To take advantage of their easy installation in outdoor or electronic applications, many epoxy–amine adhesives and coatings are cured under ambient conditions and, thus, are typically not fully cured. For these systems, changes in the environment, such as an increase in the temperature or exposure to water, can cause additional curing and can result in an increase in the physical properties; these properties can also decrease simultaneously because of plasticization. These interactions render this hygrothermal behavior complex. For such systems with complex hygrothermal behaviors, it is complicated to evaluate the behavior in that the materials properties are simultaneously influenced by two opposing effects.

In a previous study, we successfully developed a tool to evaluate these two factors separately with a model epoxy–amine system.[26] When the T_g's were measured to describe the current state of the material properties for the given system, the construction of a plot of T_g versus the conversion for the unexposed system provided an excellent method to exclude the factor of crosslink density. By applying the results of the exposed system onto this master plot, we could directly compare the T_g values between the exposed and unexposed samples while ruling out the factor of crosslink density.

In this study, we identified the complex hygrothermal behavior in two commercial epoxy products used as seal coats and impregnating resins for

Correspondence to: E. P. Douglas (edoug@mse.ufl.edu).
Contract grant sponsor: National Science Foundation Grant; contract grant number: CMS-0653969.

structural strengthening applications. As in our previous model system, T_g changed in a complicated manner because of the competing effects of both additional curing and plasticization. In this study, we focused on how to quantify those two effects separately with the master plot, using thermodynamic analysis and spectroscopic measurements.

EXPERIMENTAL

Materials

Both of the epoxy adhesive systems used in this work were used for structural strengthening applications as seal coats and impregnating resins and were purchased from Sika Corp. (Lyndhurst, NJ) and BASF (Florham Park, NJ), respectively. Each system consisted of two liquid components, where parts A and B refer to the epoxy resin component and the hardener component, respectively. In system I, part A consisted of diglycidyl ether of bisphenol A, and part B consisted of a blend of amines. In system II, part A consisted of epoxy resin, alkyl glycidyl ether, aliphatic diglycidyl ether, and ethyl benzene, whereas part B consisted of polyoxypropylene diamine, isophorone diamine, epoxy resin, benzyl alcohol, hexanediamine, and imidazole, as provided in the manufacturers' information. As suggested by the manufacturers, the mix ratios between parts A and B were 1 : 0.345 and 1 : 0.3 w/w for systems I and II, respectively.

In the sample preparation, the two liquid components were mixed vigorously for 5 min to ensure even mixing. The mixed material was then degassed for 30–60 min *in vacuo* to remove air bubbles. The specimens were cured at room temperature (RT; 22–23°C) for 4 weeks before exposure; this ensured that there was enough time for the curing reaction at RT.

Table I shows the basic thermal properties of systems I and II without any water immersion. The values of T_g and conversion were measured by differential scanning calorimetry (DSC) and Fourier transform infrared (FTIR) spectroscopy (the measurement techniques are described in the following section). As shown in Table I, the T_g values for the two systems were very close for various curing conditions; this indicated the similarity in the thermal properties between both of the unexposed systems.

TABLE I
Comparison of the Observed T_g's and Epoxide Conversion for Unexposed Systems between Systems I and II

	System I		System II	
Curing condition	T_g (°C)	Conversion	T_g (°C)	Conversion
Right after mixing	−45.9	0.00	−48.6[a]	0.00
28 days at RT	52.5	0.80	53.0	0.88
Fully cured (50°C/60 min + 80°C/120 min + 125°C/180 min)	82.1	1.00	74.2	1.00

[a] Estimated from a T_g–conversion construction.

TABLE II
Curing and Exposure Conditions for Hygrothermal Exposure in Monitoring the Changes in T_g's with DSC and Changes in the Crosslinking Density with FTIR

	Condition	Temperature (°C)	Time (days)
Curing	Air	RT	28
Hygrothermal exposure	Water immersion	30/40/50/60	1/2/4/7/14/28

The exposure environments consisted of immersion into deionized water at temperatures of 30, 40, 50, and 60°C. The details of the curing and exposure conditions for hygrothermal exposure are shown in Table II.

To construct a master plot of T_g versus the crosslink density for each system of the unexposed epoxies, we employed various curing conditions to obtain specimens with a wide range of conversion values. The specific information for the curing conditions for these specimens is shown in Table III.

Techniques

DSC (DSC 220, Seiko Instruments, Chiba, Japan) was used to identify changes in T_g with hygrothermal exposure. Samples were prepared by the deposition of a small amount of the epoxy formulation directly into the bottom of a DSC aluminum pan before the system was cured to maximize the thermal contact between the sample and the pan and to prevent the artifacts often observed during first DSC scans when there is poor thermal contact. After the sample was cured in the bottom of the pan, either the pan with the sample in it was immersed in water for hygrothermal exposure or the pan was immediately used for T_g measurement. After hygrothermal exposure, the surface of the sample was wiped carefully with a paper tissue to remove any excess surface water. The pan was immediately sealed and placed directly into the DSC chamber for measurement. To reduce the potential for any curing to occur during the measurement, T_g was determined from the first run of each specimen.

After the sample was placed in the DSC instrument, the heat flow signal was allowed to fully equilibrate before the temperature scan was begun. The temperature range for the measurement was −20 to 120–130°C at a heating rate of 10°C/min, and three replicas were run for each exposure condition to obtain an average value. T_g was chosen from the midpoint of the tangent between the extrapolated baselines before and after the transition.

TABLE III
Curing Conditions for the Master Plot of T_g versus Conversion for the Unexposed Systems I and II

Curing conditions	System I		System II	
	T_g (°C)	Epoxide conversion	T_g (°C)	Epoxide conversion
RT/0–28 days	−45.9–52.5	0.00–0.80	−48.6–53.0	0.00–0.88
80°C/110 min	59.7	0.89	56.6	0.90
90°C/80 min	65.5	0.91	66.3	0.95
90°C/110 min	76.9	0.96	—	—
50°C/60 min + 80°C/120 min + 125°C/180 min	82.1	1.00	74.2	1.00

To measure the crosslink density and the amount of absorbed water, we used FTIR spectroscopy (Nicolet Magna 760, Thermo Electron Corp., Waltham, MA) with a CaF_2 beamsplitter and an mercury cadmium telluride (MCT) detector. Near-infrared (NIR) spectra were recorded over the range 3800–7400 cm^{-1} with 32 scans at a resolution of 4 cm^{-1}. Thin films 0.5 mm thick were cast between glass plates with Teflon spacers. With the selected curing conditions, as shown in Tables II and III, the films were either immersed in water for hygrothermal exposure or directly used for the FTIR measurement.

The typical NIR spectra for each system without exposure are shown in Figure 1. The reduction in the epoxide absorbance at 4530 cm^{-1} for the higher temperature curing is evident in this figure. For the quantitative analysis of crosslink density changes, the area of the epoxide peak around 4530 cm^{-1} normalized to the phenyl peak around 4622 cm^{-1} was calculated for each system, I and II. The epoxy conversion (α) was then calculated by $\alpha = 1 - A(t)/A(0)$, where $A(t)/A(0)$ is the ratio of normalized peak area with respect to the uncured and unexposed systems. For quantitative analysis in accordance with the Beer–Lambert law, the absorbance was less than 1.0. The baselines for the area calculation of these peaks were chosen as suggested by Dannernberg[27,28] without any baseline correction.

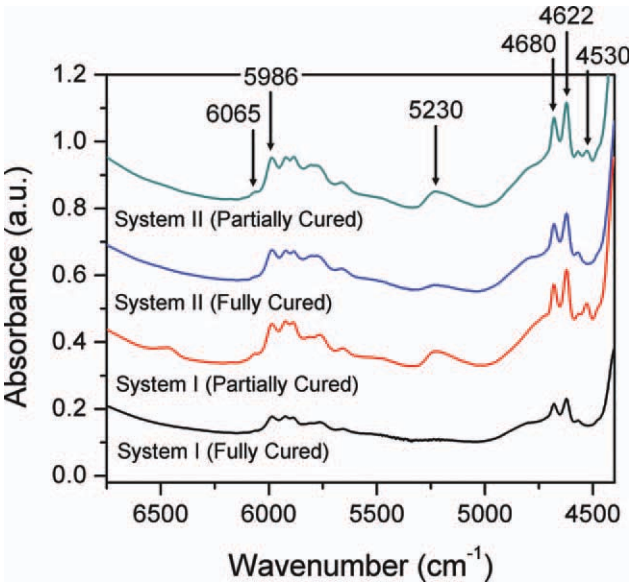

Figure 1 Typical NIR spectra for each system with different curing conditions: (from bottom to top) system I fully cured at 50°C for 1 h followed by 80°C for 2 h and 125°C for 3 h, system I partially cured at RT for 28 days, system II fully cured at 50°C for 1 h followed by 80°C for 2 h and 125°C for 3 h, and system II partially cured at RT for 28 days. [Color figure can be viewed in the online issue, which is available at wileyonlinelibrary.com.]

To estimate the amount of absorbed water for each exposure condition, the normalized area of the characteristic water peak around 5230 cm^{-1} was obtained; this was assigned to a combination of the asymmetric stretching (υ_{as}) and in-plane deformation (δ) of water.[29–31] The normalized area of the characteristic water peak provided another method to measure the amount of absorbed water in various polymer–water systems, where the normalized area was proportional to the real amount of absorbed water.[29–32] In this work, the area of this region was also normalized by the phenyl absorbance at 4622 cm^{-1}. Because these were normalized values, we could not use them to determine the absolute concentrations of water present; however, because the normalized areas were proportional to the amount of water, they could be used for relative comparisons. Although this peak included hydroxyl groups generated in the epoxy network due to the curing reaction, the change in absorbance of the peak by the curing reaction was negligible compared with the amount of absorbed water.[26]

A summary of the characteristic NIR absorption bands for systems I and II is shown in Table IV.

RESULTS

As shown in Figure 2, the DSC curves for each system after 7 days of hygrothermal exposure show that the changes in T_g were difficult to understand because of the fact that both increases and decreases in T_g were observed during the course of exposure. The samples exposed at 40, 50, and 60°C in system I showed significant increases in T_g compared with the unexposed samples, whereas T_g decreased for the

TABLE IV
Assignment of the Observed Peak for Systems I and II in the NIR Spectra

Peak position (wave number; cm^{-1})	NIR assignment
4530	Combination of C—H stretching and bending of the epoxide ring
4622, 4680	Combination of aromatic conjugated C=C stretching (1626 cm^{-1}) with aromatic CH fundamental stretching (3050 cm^{-1})
5230	Characteristic water peak by a combination of υ_{as} and δ of water
5986	Overtone of phenyl CH stretching
6065	First overtone of the terminal CH fundamental stretching

samples exposed at 30°C. On the other hand, decreases in T_g compared to the values of the unexposed samples for all of the exposure conditions were observed for system II after 7 days of exposure.

For the DSC curves in Figure 2, it is also shown that endothermic aging peaks were superimposed around the glass-transition region. This well-known behavior was structural enthalpy relaxation or physical aging, a result of the recovery of enthalpy trapped in the glassy state of the material during aging.[33–38] This phenomena is easily observed for amorphous polymers being cooled down to below T_g or being isothermally cured at a temperature below T_g; these polymers typically show enthalpy relaxation upon reheating.

To examine the changes in T_g during the entire course of exposure, the T_g's of both systems were

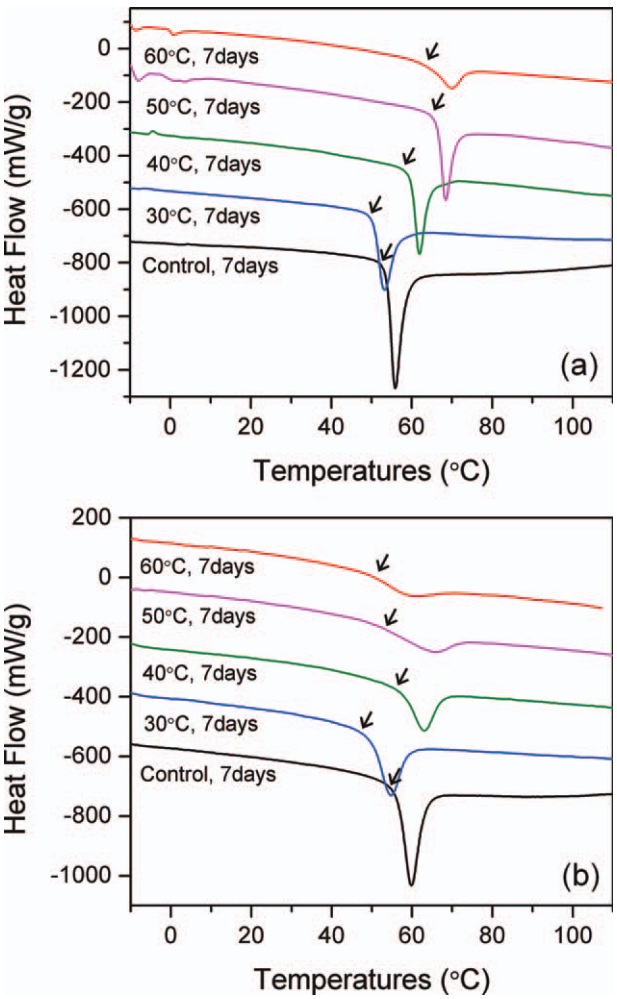

Figure 2 Typical DSC curves after water immersion for 7 days at different temperatures compared with no exposure: (a) system I and (b) system II. From the bottom of each set of DSC scans: control (exposed to air) and exposed at 30, 40, 50, and 60°C to water. The arrows indicate the T_g's for each condition. [Color figure can be viewed in the online issue, which is available at wileyonlinelibrary.com.]

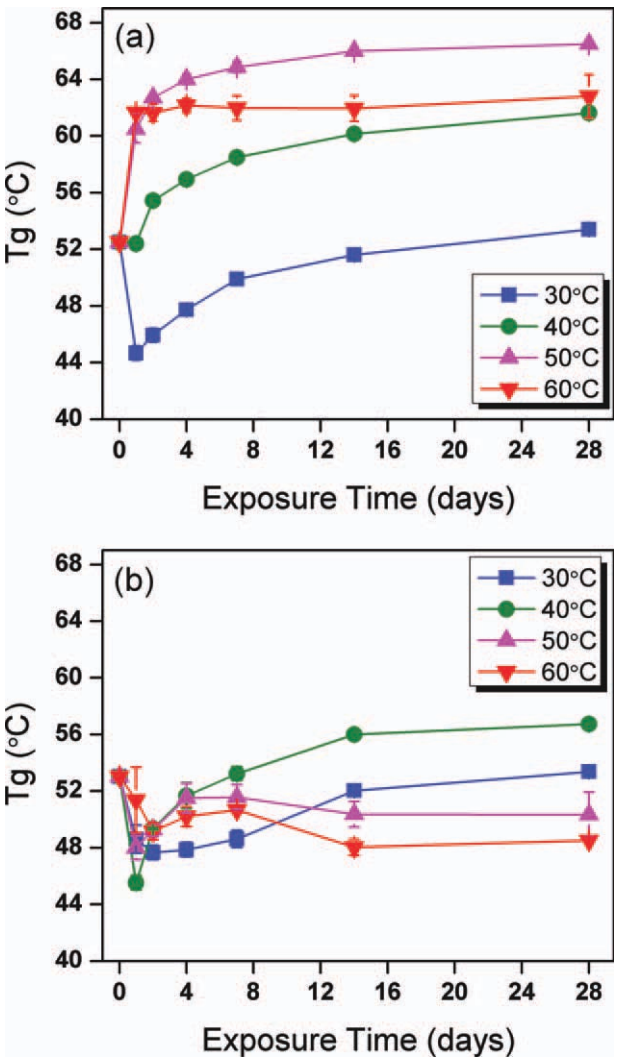

Figure 3 Changes in T_g at different exposure conditions after 4 weeks of curing at RT in air: (a) system I and (b) system II. In this picture, the size of the error bars displaying the standard deviation is too small to be shown at some points. [Color figure can be viewed in the online issue, which is available at wileyonlinelibrary.com.]

plotted as a function of the exposure time, as shown in Figure 3. The results clearly indicate complex hygrothermal behavior, in that both an increase and a decrease in T_g were observed during the course of exposure. However, each system exhibited a different behavior in terms of the manner of the changes in T_g for each exposure condition. For system I, the samples exposed at 50 and 60°C showed continuous increases in T_g with exposure until the rates of increase slowed down and approached saturation points, whereas for the samples exposed at 30 and 40°C, an initial decrease in T_g was followed by an increase. On the other hand, for system II, the T_g values for all of the exposure conditions initially decreased in the beginning stage of exposure but then increased after 1–2 days of exposure. In the later stage of exposure, the samples exposed at 30 and 40°C continued to show an increase in T_g until the rates of increase slowed down and approached saturation points. On the contrary, samples exposed at 50 and 60°C exhibited an additional decrease of T_g in the later stage and approached saturation points.

To determine how the postcuring reactions affected the hygrothermal behavior, changes in the conversion in terms of the decrease in epoxide groups were also monitored during the exposure. The curing conditions in this experiment were the same as those used to measure the changes in T_g, namely, 4 weeks at RT in air before the exposure was started. As shown in Figure 4, for the samples exposed to water immersion for 7 days at different temperatures were compared with control samples that had been exposed to air for 7 days, there was clearly a decrease in the area for the epoxide groups around 4530 cm^{-1} with an increase in the exposure temperature; this indicated that a postcuring reaction obviously occurred.

By monitoring the changes in conversion during the entire course of exposure, as shown in Figure 5, we clearly observed that the epoxide conversion in both systems increased because of the postcuring reaction for all of the exposure conditions; this resulted in significant increases in the crosslink density (10–20%) compared with the unexposed sample. This result shows that the elevated temperature of the water caused additional curing, even at a low temperature, such as 30°C.

A comparison of the changes in T_g and the conversion with hygrothermal exposure for each system (Figs. 3 and 5) clearly indicated that the increase in the crosslink density by the postcuring reaction led to an increase in T_g with exposure. At the same time, property loss by plasticization simultaneously occurred with additional curing; this also played a significant role in determining the properties. It was evident that the two phenomena were in competition with each other during the exposure.

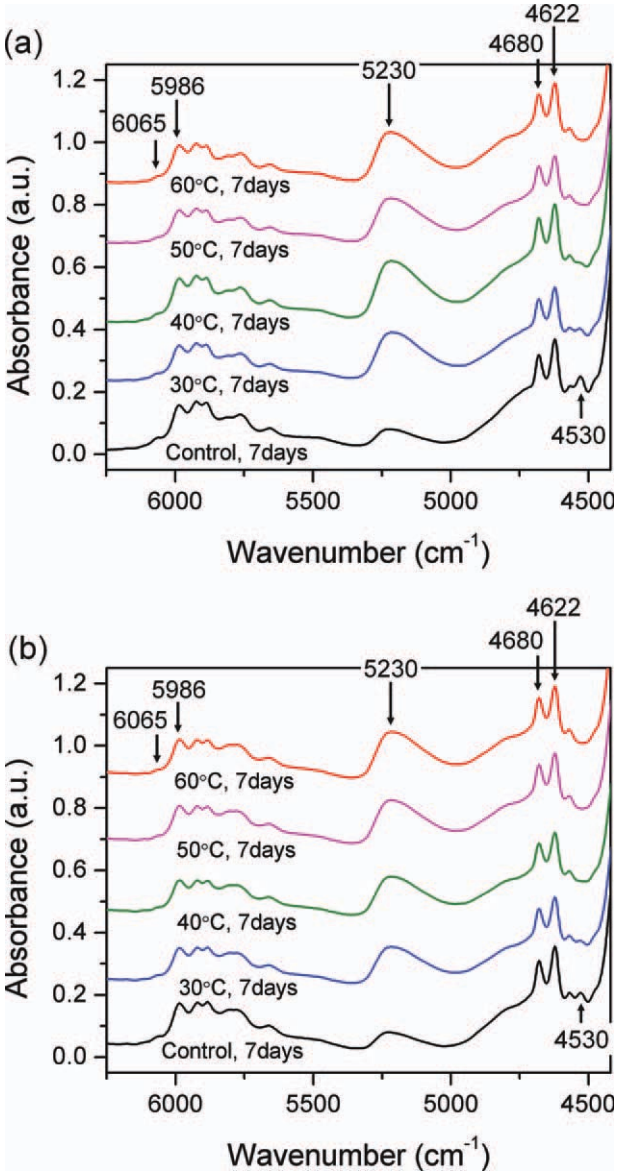

Figure 4 NIR spectra for samples immersed in water for 7 days at different temperatures compared with an unexposed control sample: (a) system I and (b) system II. From the bottom of each set of FTIR spectra: control (exposed to air) and exposed at 30, 40, 50, and 60°C to water. The curing conditions were 4 weeks at RT in air before the exposure was started. [Color figure can be viewed in the online issue, which is available at wileyonlinelibrary.com.]

For example, in system I, the samples exposed at 30 and 40°C showed an initial decrease in T_g, despite a continuous increase in the crosslink density; this indicated that the plasticization effect by water had the predominant effect on T_g in the initial stage compared with additional curing. However, as exposure was continued, the additional curing became the dominating factor, resulting in an increase in T_g. With regard to the exposure at 50°C, it was observed that the increase in the crosslink density was dominant throughout the exposure and resulted in a monotonic increase in T_g. When we compared the

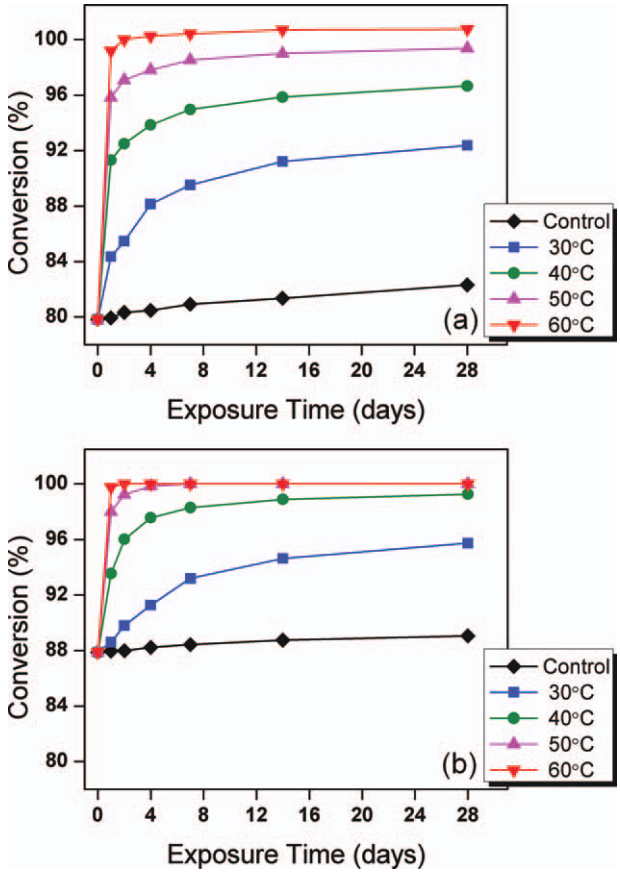

Figure 5 Changes in the conversion at different exposure conditions after 4 weeks of curing at RT in air: (a) system I and (b) system II. [Color figure can be viewed in the online issue, which is available at wileyonlinelibrary.com.]

samples at 50 and 60°C, the T_g for the 50°C samples was larger than the T_g for the 60°C samples after 1 day of exposure, even though the samples exposed at 60° always had a higher conversion value. This indicated that at 60°C, there was more absorbed water and, therefore, greater plasticization.

In a similar manner, system II also shows the combined effect of the two competing factors during exposure. The samples exposed at 30 and 40°C showed initial decreases in T_g; this indicated a larger plasticization effect, which was dominant over the effect of additional curing, followed by increases in T_g's, which indicated a change in the dominating factor from plasticization to additional curing. For the samples exposed at 50 and 60°C, it was shown that the dominating factor was changed from plasticization in the initial stage (causing decreases in T_g at 1–2 days of exposure) to additional curing in the middle stage (causing increases in T_g at 2–7 days of exposure) and back to plasticization later (causing decreases in T_g at 7–14 days of exposure). In this system, the larger plasticization effect was also observed at higher temperatures of exposure, in which the samples exposed at 50 and 60°C showed lower T_g values than those exposed at 30 and 40°C in the later stage of exposure despite higher conversion values.

DISCUSSION

From the comparison of the two figures showing changes in T_g and conversion with hygrothermal exposure (Figs. 3 and 5), we can see that the increase in T_g due to additional curing and the decrease in T_g due to plasticization were in competition with each other during exposure. In our previous study, we successfully developed a tool for the evaluation of the relative importance of these two effects separately, in which T_g for the unexposed system was plotted as a function of conversion. We could then use this master plot to exclude the influence of the crosslink density by plotting the results from Figures 3 and 5 onto this master plot, making it possible to compare the T_g values directly between the exposed and unexposed systems at the same conversion value.

For the construction of the T_g–conversion master plot, the well-known semiempirical expression for the relationship between T_g and conversion for crosslinked systems was used as follows:[39–41]

$$\ln(T_g) = \frac{(1-\alpha)\ln(T_{g0}) + (\Delta C_{p\infty}/\Delta C_{p0})\alpha \ln(T_{g\infty})}{(1-\alpha) + (\Delta C_{p\infty}/\Delta C_{p0})\alpha}$$

where T_{g0} and $T_{g\infty}$ are the T_g values of the monomer and the fully cured network and ΔC_{p0} and $\Delta C_{p\infty}$ are the heat capacity changes at T_{g0} and $T_{g\infty}$, respectively.

To construct the master plot of T_g as a function of conversion, T_g and conversion values under identical curing conditions were experimentally obtained for unexposed samples of each system. The previous semiempirical equation was used to fit the experimentally obtained data, as shown in Figure 6. Both systems showed good agreement with the experimental data, with coefficients of determination of 0.99 for both cases. The values of $\Delta C_{p\infty}/\Delta C_{p0}$ as a fitting parameter were 0.88 and 0.66 for systems I and II, respectively.

In the construction of the master plot for system II, the samples with lower values of conversion exhibited multiple T_g values in the DSC curves; this might have been due to phase separation between the epoxy resin and the hardener. Because system II consisted of a blend of different amines, it is possible that the system under a low value of conversion still had phase separation after hand mixing, which resulted in multiple T_g's. This behavior, however, disappeared for conversions of 0.23 and higher, where there was a single value of T_g. Thus, for

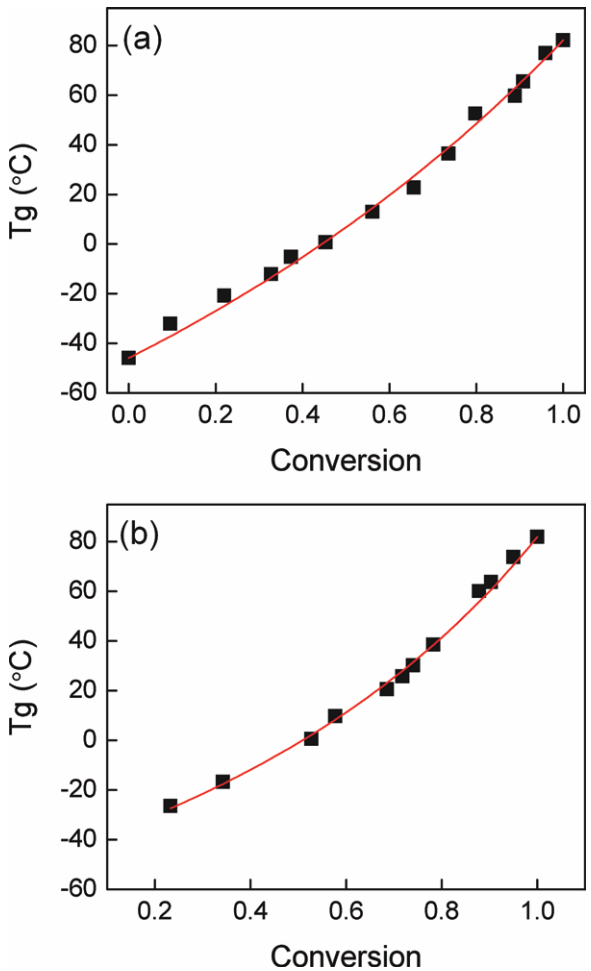

Figure 6 T_g versus the conversion master plot for unexposed systems: (a) system I and (b) system II. The points were experimentally obtained, and the solid lines are fitted to the theoretical data. [Color figure can be viewed in the online issue, which is available at wileyonlinelibrary.com.]

system II, samples with conversion values greater than 0.23 were used to construct the master plot. On the contrary, system I did not exhibit phase separation of the initial epoxy/hardener mixture; this indicated that the blend of amines used in this product was well-mixed even before curing. Because T_g for the uncured system II could not be measured experimentally, we estimated T_{g0} for system II by fitting the semiempirical equation shown previously, and the value was −48.6°C.

Into these master plots for the unexposed systems, the values of T_g and conversion for each exposed system, I and II, shown in Figures 3 and 5, were finally applied, as displayed in Figures 7 and 8. In these figures, the difference in the glass-transition temperatures between the unexposed and exposed samples at the same conversion value (ΔT_g) could be used as a parameter indicating the plasticization effect quantitatively whereas excluding the influence of changes in the crosslink density with exposure. In this calculation of ΔT_g, T_g's of the exposed system were determined directly from DSC measurements, whereas the T_g values at the corresponding conversions for the unexposed system were obtained from the values on the fitted curve, as indicated in Figures 7(b) and 8(b).

To correlate ΔT_g with the absorbed water amount at each exposure condition, the relative amount of water uptake was determined from the characteristic water peak around 5230 cm^{-1}, which was well resolved in the NIR spectra of each system. When the relative amount of absorbed water was evaluated by this method, both systems exhibited the same typical trends in that the amount of water absorbed increased as the exposure continued and the rate of increase in absorbed water at the initial stage of the exposure was enhanced as the exposure temperature

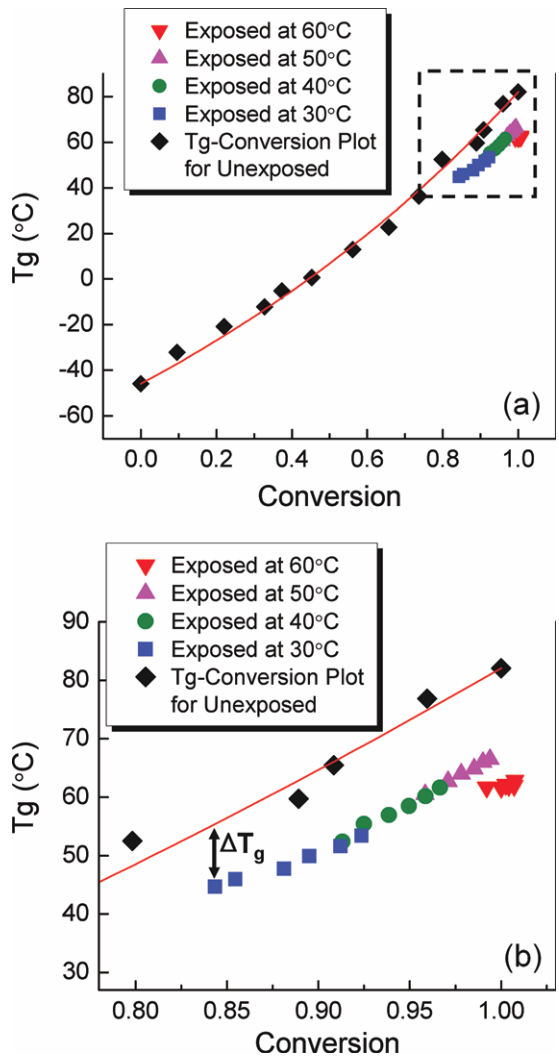

Figure 7 Direct comparison of T_g between the unexposed and exposed samples for system I with the master plot of T_g versus conversion. The section marked with dotted lines in part a is magnified in part b. [Color figure can be viewed in the online issue, which is available at wileyonlinelibrary.com.]

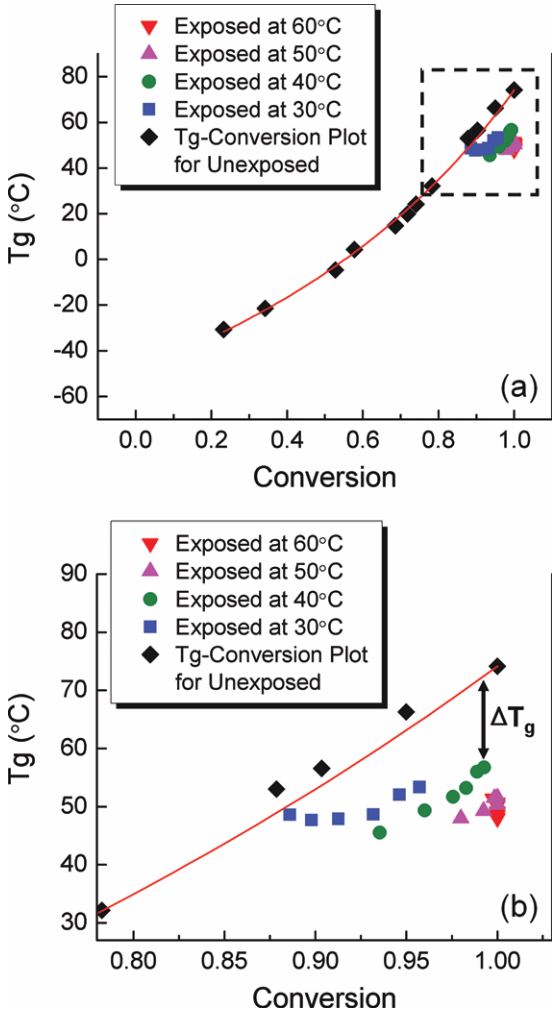

Figure 8 Direct comparison of T_g between the unexposed and exposed samples for system II with the master plot of T_g versus conversion. The section marked with dotted lines in part a is magnified in part b. [Color figure can be viewed in the online issue, which is available at wileyonlinelibrary.com.]

was increased because of an increase in the diffusion rate as the temperature was increased.

However, the examination of the amount of water absorbed in the later stages of exposure showed that the two systems exhibited different behaviors as a function of the exposure temperature. For system II, the amount of water absorbed after saturation increased as the exposure temperature was increased, as expected. However, for system I, the amount of water absorbed after saturation decreased as the exposure temperature was increased. This anomalous behavior may have been due to the imperfect curing of system I.[42] The degree of conversion varied significantly as a function of exposure temperature for system I; this resulted in a significant difference in the network structure. We speculate that the looser network, which resulted from the lower crosslink density at lower exposure temperatures, allowed for the easier diffusion of water and resulted in greater amounts of absorbed water for samples exposed at lower temperatures. In contrast, system II showed a much lower difference in conversion for different exposure temperatures. In addition, the conversion for system II was generally higher than that of system I under the same exposure conditions; this resulted in a tighter network. Thus, the difference in network structure was not as great for system II; this made the temperature the dominant factor in determining the water absorption (Fig. 9).

The amount of water absorption at equilibrium was influenced not only by the water temperature or the free volume in the polymer matrix but also by the number of polar functional groups forming hydrogen bonds between water and the polymer network. Because previous studies have suggested that water molecules mostly bond to polar groups,[43–45] the total amount of water absorption at equilibrium could have depended on the number of polar functional groups available for the water

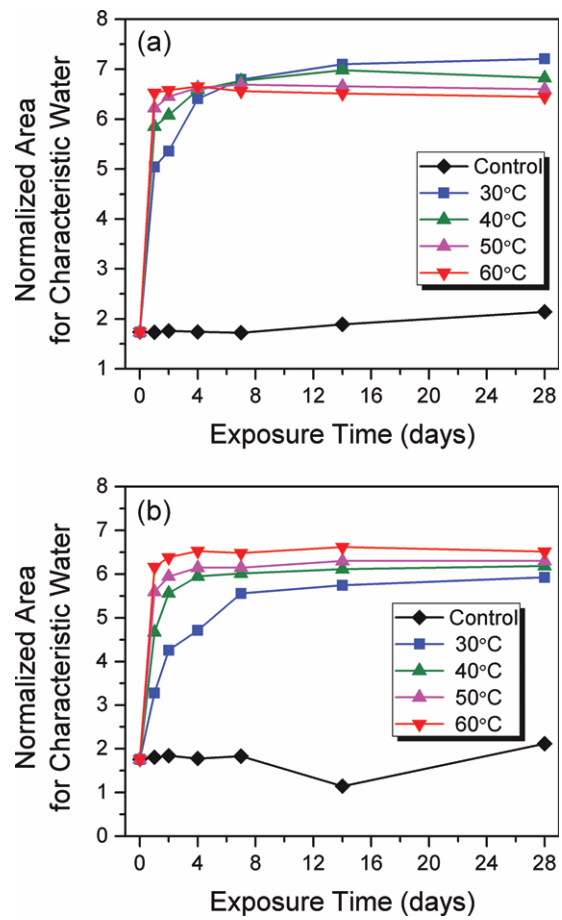

Figure 9 Relative amount of water absorption with the exposure time estimated by the normalized area of the characteristic water peak from NIR: (a) system I and (b) system II. [Color figure can be viewed in the online issue, which is available at wileyonlinelibrary.com.]

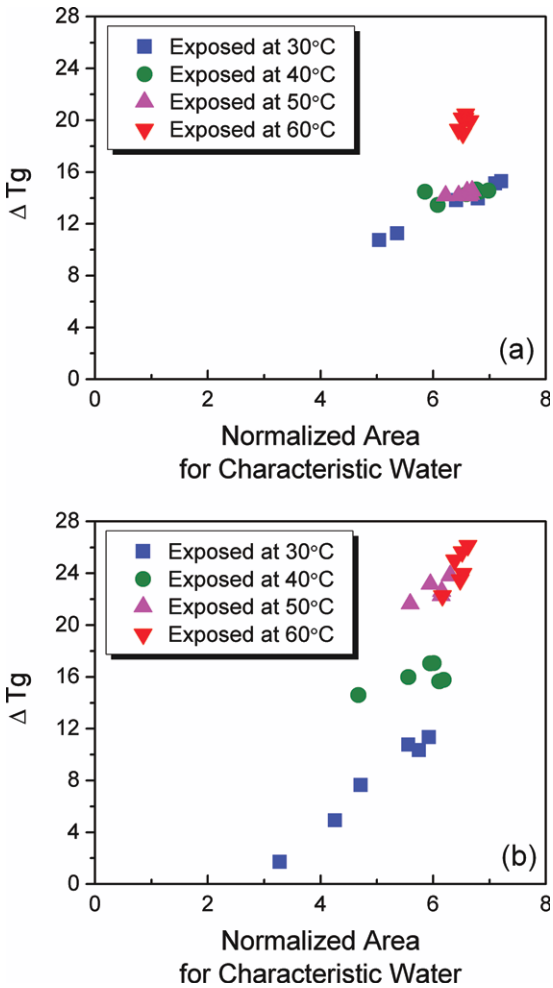

Figure 10 ΔT_g's between the unexposed and exposed systems as a function of the estimated amount of absorbed water: (a) system I and (b) system II. [Color figure can be viewed in the online issue, which is available at wileyonlinelibrary.com.]

molecules, in which more functional groups resulted in higher diffusion coefficients.

In the epoxy systems examined in this study, the possible effect of such polar functional groups needed to be considered as a possible explanation for the anomalous behavior of system I described previously, where the amount of water absorbed after saturation decreased as the exposure temperature was increased because of the greater postcuring at higher exposure temperatures. However, with regard to the degree of curing at different exposure temperatures after saturation was reached, Figure 5(a) shows that the specimens exposed at higher temperatures always showed a higher degree of conversion than those exposed at lower temperatures and thus had more hydroxyl functional groups. Despite the greater number of hydroxyl groups, the systems exposed at higher temperatures had lower equilibrium water uptake; this confirmed that the effect of the difference in network with different temperatures was the dominant factor in determining the equilibrium water absorption.

Finally, ΔT_g was plotted as a function of the relative absorbed water amount for each exposure system. As shown in Figure 10, ΔT_g increased with water amount; this was the expected behavior of the increase in plasticization as the amount of absorbed water increased. In a comparison of the two systems in this figure, system II showed a larger slope; this indicated that small changes in the water absorption resulted in larger plasticization in this system.

CONCLUSIONS

In this work, the complex hygrothermal behavior of two commercial epoxy products, both used as seal coats and impregnating resins for structural strengthening applications, were investigated. In both of these systems, property loss by plasticization simultaneously occurred with additional curing during exposure.

From the comparison of the changes in T_g and crosslink density with water immersion at different temperatures, it was clear that the plasticization effect due to water absorption and the effect of additional curing due to the postcuring reaction were in competition with each other during exposure.

The construction of the plot of T_g versus conversion for the unexposed system provided an excellent method for excluding the factor of crosslink density in understanding the hygrothermal behavior. By applying the results for the exposed system onto this master plot, we could directly compare the T_g values between the exposed and unexposed samples while ruling out the factor of crosslink density. Combined with the estimated amounts of water absorption, this provided a tool for quantitatively evaluating the plasticization effect due to environmental exposure.

This method could be used to understand the complex behavior of various crosslinked polymer systems that are cured at low temperatures and used in applications where they are exposed to the environment.

References

1. Blanco, I.; Cicala, G.; Costa, M.; Recca, A. J Appl Polym Sci 2006, 100, 4880.
2. Ren, S. P.; Liang, L. Y.; Lan, Y. X.; Lu, M. G. J Appl Polym Sci 2007, 106, 2917.
3. Crivello, J. V.; Narayan, R. Macromolecules 1996, 29, 433.
4. Chen, J. S.; Ober, C. K.; Poliks, M. D.; Zhang, Y.; Wiesner, U.; Cohen, C. Polymer 2004, 45, 1939.
5. Ding, Y.; Liu, M.; Li, S.; Zhang, S.; Zhou, W. F.; Wang, B. Macromol Chem Phys 2001, 202, 2681.
6. Deneve, B.; Shanahan, M. E. R. Polymer 1993, 34, 5099.
7. Xiao, G. Z.; Delamar, M.; Shanahan, M. E. R. J Appl Polym Sci 1997, 65, 449.

8. Xiao, G. Z.; Shanahan, M. E. R. J Appl Polym Sci 1998, 69, 363.
9. Perrin, F. X.; Nguyen, M. H.; Vernet, J. L. Eur Polym J 2009, 45, 1524.
10. LaPlante, G.; Lee-Sullivan, P. J Appl Polym Sci 2005, 95, 1285.
11. Nunez, L.; Villanueva, M.; Fraga, F.; Nunez, M. R. J Appl Polym Sci 1999, 74, 353.
12. Apicella, A.; Nicolais, L. Adv Polym Sci 1985, 72, 69.
13. Yang, Q.; Xian, G.; Karbhari, V. M. J Appl Polym Sci 2008, 107, 2607.
14. Lu, M. G.; Shim, M. J.; Km, S. W. J Appl Polym Sci 2001, 81, 2253.
15. Nogueira, P.; Ramirez, C.; Torres, A.; Abad, M.; Cano, J.; Lopez, J.; Lopez-Bueno, I.; Barral, L. J Appl Polym Sci 2001, 80, 71.
16. Jelinski, L. W.; Dumais, J. J.; Cholli, A. L.; Ellis, T. S.; Karasz, F. E. Macromolecules 1985, 18, 1091.
17. Zhou, J.; Lucas, J. P. Polymer 1999, 40, 5505.
18. Gupta, V. B.; Drzal, L. T.; Rich, M. J. J Appl Polym Sci 1985, 30, 4467.
19. Maggana, C.; Pissis, P. J Polym Sci Part B: Polym Phys 1999, 37, 1165.
20. Vanlandingham, M. R.; Eduljee, R. F.;Gillespie J. W. J Appl Polym Sci 1999, 71, 787.
21. Wu, L.; Hoa, S. V.; Minh-Tan, T.-T. J Appl Polym Sci 2006, 99, 580.
22. Devasahayam, S. J Appl Polym Sci 2006, 99, 3318.
23. Thomson, K. W.; Wong, T.; Broutman, L. J Polym Eng Sci 1984, 24, 1270.
24. Netravali, A. N.; Fornes, R. E.; Gilbert, R. D.;Memory J. D. J Appl Polym Sci 1985, 30, 1573.
25. Johncock, P. J Appl Polym Sci 1990, 41, 613.
26. Choi, S.; Douglas, E. P. Am Chem Soc Appl Mater Interfaces 2010, 2, 934.
27. Dannenberg, H. Soc Plast Eng Trans 1963, 3, 78.
28. Chike, K. E.; Myrick, M. L.; Lyon, R. E.; Angel, S. M. Appl Spectrosc 1993, 47, 1631.
29. Musto, P.; Ragosta, G.; Mascia, L. Chem Mater 2000, 12, 1331.
30. Musto, P.; Ragosta, G.; Scarinzi, G.; Mascia, L. J Polym Sci Part B: Polym Phys 2002, 40, 922.
31. Musto, P.; Mascia, L.; Ragosta, G.; Scarinzia, G.; Villano, P. Polymer 2000, 41, 565.
32. Fukuda, M.; Kawai, H.; Yagi, N.; Kimura, O.; Ohta, T. Polymer 1990, 31, 295.
33. Fraga, F.; Castro-Diaz, C.; Rodriguez-Nunez, E.; Martinez-Ageitos, J. M. Polymer 2003, 44, 5779.
34. Ribas, S. M. Prog Colloid Polym 1992, 87, 78.
35. Shi, X.; Fernando, B. M. D.; Croll, S. G. J Coat Technol Res 2008, 5, 299.
36. Bockenheimer, C.; Fata, D.; Possart, W. J Appl Polym Sci 2004, 91, 369.
37. Montserrat, S.; Cortes, P.; Calventus, Y.; Hutchinson, J. M. J Therm Anal 1997, 49, 79.
38. Fraga, F.; Payo, P.; Rodriguez-Nunez, E.; Martinez-Ageitos, J. M.; Castro-Diaz, C. J Appl Polym Sci 2006, 103, 3931.
39. Wise, C. W.; Cook, W. D.; Goodwin, A. A. Polymer 1997, 38, 3251.
40. Couchman, P. R.; Karasz, F. E. Macromolecules 1978, 11, 117.
41. Pascault, J. P.; Williams, R. J. J. J Polym Sci Part B: Polym Phys 1990, 28, 85.
42. Abdelkader, A. F.; White, J. R. J Appl Polym Sci 2005, 98, 2544.
43. Mijovic, J.; Zhang, H. Macromolecules 2003, 36, 1279.
44. Mijovic, J.; Zhang, H. J Phys Chem B 2004, 108, 2557.
45. Soles, C. L.; Chang, F. T.; Bolan, B. A.; Hristov, H. A.; Gidley, D. W.; Yee, A. F. J Polym Sci Part B: Polym Phys 1998, 36, 3035.